



Modifying TiO₂ nanotube using N-doping and electrochemical reductive doping as a supercapacitor electrode

Faezeh Ghorbani, Shahin Khameneh Asl*

Department of Materials Engineering, Faculty of Mechanical Engineering, University of Tabriz, Tabriz, Iran.

Received: 24 August 2021; Accepted: 26 October 2021

*Corresponding author email: Khameneh@tabrizu.ac.ir

ABSTRACT

The relatively small specific capacitance along with poor electrochemical activity and weak electrical conductivity of TiO₂ has resulted in several studies on the methods of modifying TNTs (TiO₂ nanotube arrays). In this study, different mechanisms for improving the electrochemical properties of TiO₂ nanotubes are employed; Nitrogen doping of TNTs in different concentrations of ammonia solution (named N-TNTs), then conducting electrochemical reductive doping on optimized TNTs (named N-R-TNTs). Nitrogen doping of TNTs fabricated using two-step anodization was used to narrow the bandgap of TNTs as a non-metal doping technique. To better demonstrate the impact of the nitrogen content on enhancing the electrochemical activity, TNTs were immersed in 0.5, 1, 2, 4, and 8 molars of ammonia solution. Electrochemical reductive doping was implemented on TNTs and N-TNTs. The phase structure and surface morphologies of the as-prepared TNTs were identified by X-ray diffraction (XRD), Field Emission Electron Microscope (FESEM) and Fourier transformed infrared spectroscopy (FT-IR) measurements. The electrochemical response of the TNTs following nitrogen and electrochemical doping was evaluated using cyclic voltammetry (CV), galvanostatic charge-discharge tests, and electrochemical impedance spectroscopy (EIS). The electrochemical measurements of the modified samples confirmed that a noticeable improvement was achieved in the electrochemical behavior and that the areal capacitance of R-N-TNT was roughly 400 orders of magnitude greater than that of TNTs with long-term stability (93% of its initial capacitance after 500 cycles).

Key words: TiO₂ nanotube, supercapacitor, modifying, capacitance performance

1. Introduction

Among the various energy conversion and storage devices, batteries and supercapacitors are the most commonly utilized systems. Supercapacitors are widely used as sources of energy in electrical/hybrid vehicles, portable electronic devices, and other energy backup systems. Among the diverse energy conversion and storage systems, supercapacitors have attracted a great deal of attention due to their high power density, long lifecycle, and short charge-discharge time that make them an appropriate choice for such

applications. A supercapacitor device consists of two electrodes, the electrolyte and a separator that electrically isolates the two electrodes. To obtain high specific capacitance, the electrode material must possess high surface area and good electronic conductivity [1].

Based on charge storage mechanisms, supercapacitors are generally classified into two categories, electrochemical double-layer capacitors (EDLCs) and pseudocapacitors. EDLCs (known as non-faradic) are based on charge separation at the electrolyte-electrode interface, while

pseudocapacitors chemically store their charge via redox reaction at the vicinity of the surface electrode material [2].

Materials such as activated carbon [3] graphene [4], and carbon nanotubes [5] are studied as EDLCs and transition metal oxides such as RuO₂ [6], Co₃O₄ [7], NiO [8] and MnO₂ [9] act as pseudocapacitor electrodes.

In comparison, pseudocapacitors exhibit a higher energy density and specific capacitances compared to EDLCs, while pseudocapacitors often display weak cyclic stability. Moreover, owing to the reduced reversibility faradic process, these kinds of electrodes suffer from a lower power density [10].

Many different materials have been tested as electrodes in supercapacitor applications. One-dimensional nanostructures such as nanotubes provide pathways for unidirectional and rapid electron transport, thus improving the ion absorption can enhance the speed of surface redox reactions. As a result, these structures can be utilized as supercapacitor electrodes [2,11]. Special properties of TiO₂ nanotubes including relatively high capacity, a low self-discharge rate, chemical stability, environmental benignity, and low cost render them an appropriate candidate as anode materials for supercapacitors [12]. Despite their excellent morphological structure and surface area, the synthesized TNTs exhibit negligible capacitance (less than 1 mF cm⁻²) [13]. Since TiO₂ is a wide-bandgap semiconductor (3.2 eV for anatase and 3.0 eV for rutile), it suffers from a brittle phase and poor conductivity. Also, as a supercapacitor electrode, it is countered with limited flexibility and a low specific capacitance [14].

Among the different phases of TiO₂, rutile possesses the highest thermodynamical stability, while anatase is preferred due to its larger bandgap and higher conduction band edge [15].

Along with the various other techniques of synthesizing TiO₂ nanotubes such as hydrothermal [16], spray pyrolysis [17], electrospinning [18], electrochemical anodization [19], and chemical treatment of fine TiO₂ nanoparticles [20], anodization has garnered a great deal of popularity due to its facile, and low-cost process involved. However, the semiconductor nature of TiO₂ NTs often leads to low electrochemical activity and poor conductivity, so that in the case of high-performance supercapacitors, TNTs are more restricted [21]. Thermal treatments, hydrogenated processes, chemically or electrochemically self-

doped methods are among the approaches employed to improve the electrochemical behavior of the TNTs [22]. Introducing metal [23] or nonmetal impurities into the oxide [24] to generate donor or acceptor states in the bandgap for increasing the focus of charge carriers can enhance the electrical conductivity of TiO₂.

Studies have been undertaken on the nonmetal doping method for enhancing the electrochemical activity of TiO₂ using nitrogen, carbon, sulfur, boron, and phosphorus. Among the mentioned materials, nitrogen is more attractive as it exhibits small ionization energy, comparable atomic size with oxygen, has a metastable center, and can narrow the bandgap of TiO₂ [2].

The electrochemical doping process is one of the simplest techniques of enhancing the electrical properties of TiO₂ nanostructures, as no expensive facilities, high processing temperatures, or longer process times are required [26]. As a result, Ti⁴⁺ is reduced to Ti³⁺ via electron transfer from the cathode to form a better conductive layer at the bottom, subsequently enhancing the conductivity of the nanotube. TiO₂ can then be modified at ambient temperature through an electrochemical doping process [1,27].

In this study, different mechanisms for improving the electrochemical properties of TiO₂ nanotubes are investigated. For this purpose, TiO₂ NTAs fabricated through anodization were converted into crystalline form by annealing treatment. Then, the samples were immersed in different concentrations of NH₃-H₂O solution followed by annealing in a muffle furnace for 2 h. Following the optimization of nitrogen extent, electrochemical doping processes were utilized as a simple and fast method of modifying TNTs. CV, EIS, as well as charge and discharge tests were carried out on the samples titled TNT (unmodified), N-TNT, R-TNT, and R-N-TNT to compare the impact of modification mechanisms on the capacitance performance.

2. Experimental

2.1. Preparation of Titania Nanotubes

High-purity titanium commercial sheets (Gr. 2, 99.7%, 0.5 mm) were cut into dimensions of 1*2 cm². They were then being polished with grade 100 up to 1500 emery papers, and then mechanically polished using 0.05 mm Al₂O₃ powder. The samples were later degreased using sonication in acetone and ethanol for 15 min. For the synthesis of TiO₂ nanotube arrays, a two-step anodization

procedure was carried out. For this purpose, the anodizing electrolyte consisted of ethylene glycol ($C_2H_6O_2$), 0.15M NH_4F , and 3 vol% DI water. First stage anodization was configured for a two-electrode cylindrical setup consisting of Ti samples as anode and stainless steel as cathode for 2 hours at 30° C. The cell voltage was set at 60 v, and the distance between the anode and cathode was 2 cm. Subsequently, the formed titanium oxide layer was ultrasonically removed using deionized water. The second stage anodization was carried out under the same conditions, but with an anodization time of 4 hours instead.

2.2. Synthesis of N-doped TiO_2 nanotube arrays

For the synthesis of the N-doped TiO_2 NTAs, the as-prepared samples were immersed in different densities of $NH_3 \cdot H_2O$ solution (0.5, 1, 2, 4, 8 M) for 15 h in a covered case, and then rinsed with DI water. To achieve the anatase phase, samples were annealed in air at 500 °C for 3 hours under a specific heating rate. To get better capacitive improvement results, the optimized samples were exposed to electrochemical reductive doping (R-N-TNT). For the sake of better comparison, electrochemically doped TNT (H-TNT) was also synthesized, which shall be discussed in the later sections.

2.3. Electrochemical doping of N-doped Titania Nanotubes

The electrochemical doping of N-TNTs was performed within the same two-electrode electrochemical cell, with N-TNTs acting as cathode and high-density graphite electrode as the anode. 0.5M Na_2SO_4 (MERCK) was used as a

supporting electrolyte. Electrochemical Reduction doping was carried out at 5 v for 30 sec.

2.4. Material Characterization and Electrochemical Measurements

The electrochemical performance of the prepared samples was evaluated by cyclic voltammetry (CV), galvanostatic charge-discharge tests, and electrochemical impedance spectroscopy (EIS); using a potentiostat galvanostat Wonatech ZIVE module in 0.5M Na_2SO_4 solution as the supporting electrolyte. All of the electrochemical analyses were carried out using a three-electrode cell system, in which a platinum sheet, a calomel electrode, and the prepared samples acted as counter, reference, and working electrodes, respectively. All EIS tests were performed at an open-circuit voltage within the frequency range of 100 kHz to 1 mHz, and all the CV tests were conducted at the potential range of -0.2 to 1 volt. The morphology and the microstructure of the samples were characterized using MIRA3 TESCAN FESEM apparatus. The chemical composition of metal oxide samples was studied by X-ray photoemission spectroscopy using D-5000 Siemens with Cu source. Fourier transform infrared spectra (FTIR) of the samples were obtained using FTIR-8400S SHIMADZU apparatus.

3. Results and discussion

Electrochemical impedance spectrometry is employed to evaluate the conductivity of Nitrogen-doped TNT samples under different concentrations. Fig. 1 illustrates the Nyquist representation of EIS data collected at OCP. As can be observed, the

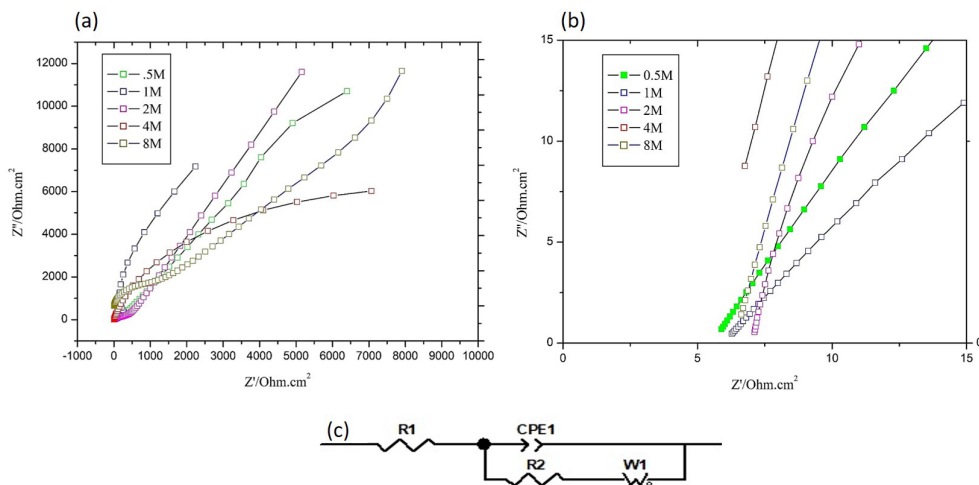
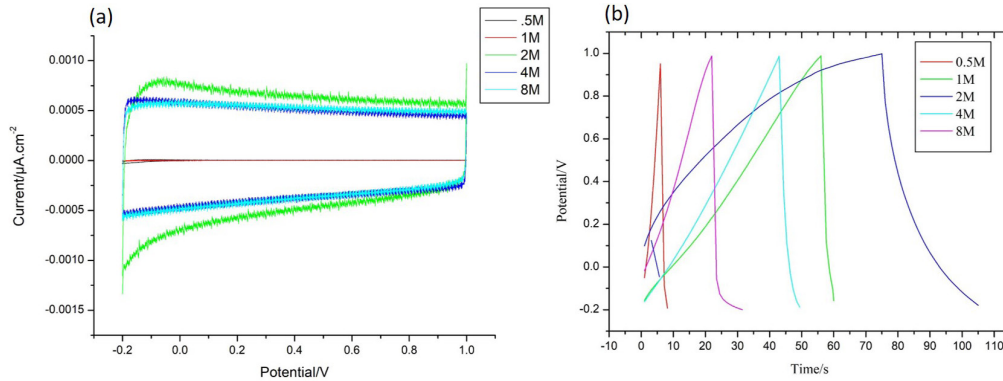


Fig. 1- Nyquist plots of EIS data collected at 0.5 M Na_2SO_4 for (a) 0.5, 1, 2, 4, 8 M N-doped samples and (b) the magnified high-frequency region of the same plots. (C) Representation the applied equivalent circuit.

Table 1- The fitting values obtained from the equivalent circuit in Fig. 1

sample	.5M	1M	2M	4M	8M
$R_1(\Omega.cm^{-2})$	5.547	5.979	7.045	5.092	6.351
$CPE1-T(mFs^p.1cm^{-2})$	0.00010181	0.00039351	8.5065E-6	8.7737E-7	5.721E-6
$CPE1-P$	0.70846	0.63248	0.9197	0.88064	.87656
$R_{ct}(\Omega.cm^{-2})$	361.5	189.1	76.2	11560	937.7
$W-R(\Omega.cm^{-2})$	49447	126.1	1024	1.2837E5	20436
$W-T$	56.46	0.82681	0.44495	69.6	101334
$W-P$.68329	0.64746	0.37541	0.41428	0.0039257

Fig. 2- (a) CV and (b) galvanostatic charge/discharge curves under a current density of 50 μA for 0.5, 1, 2, 4, 8 M N-doped samples.

impedance plots for the 2 M N-doped sample have more vertical plots and also exhibit much a higher impedance value than the other samples, which is related to their ideal capacitor behavior. Moreover, the curve of the 2 M N-doped sample possess a smaller semicircle over the high-frequency range indicating a higher conductivity. Previous studies have reported the impact of N-dopant at lowering the surface resistance of TNTs [27]. To obtain better results, the amount of N-dopant needs to be optimized. Table 1 lists the correlation between the parameters of the equivalent circuits, in which R_1 is electrolyte resistance, C is the Helmholtz double-layer capacitance of TNT arrays, CPE is the constant phase element and R_{ctc} relates to the interface of charge transfer resistance. Owing to the usage of the 2 M Li_2SO_4 solution as the test solution, the value of R_1 (solution resistance) is similar for all the samples. Warburg resistance of the 2M sample is the least, however, the CPE value of this sample is higher than the rest. The magnitude of R_{ctc} for the 2 M N-doped sample is at a minimum ($76.2 \Omega.cm^{-2}$), which represents faster charge transfer compared to the 0.5, 1, 4, and 8 M samples.

Fig. 2a depicts CV curves of the N-doped samples implemented at $100 mV.s^{-1}$ scan rate. According to the figure, all the samples feature ideal rectangular shapes without noticeable signs of redox peaks, which can be ascribed to the

double-layer capacitance behavior. Moreover, the cv curve of the 2 M N-doped sample possesses the largest integrated area, indicating the enhancement of capacitance behavior. The areal capacitance obtained from the CV curves at $100 mA.cm^{-1}$ can be calculated according to the equations (1) [28]:

$$C_s = \int (I \cdot dv) / S \cdot v \cdot V \quad (1)$$

In which C_s is the areal capacitance ($mF.cm^{-2}$), I is the current (A), v is the scanning rate ($mA.cm^{-1}$), and V is the potential (V) S is the surface area of the working electrode (cm^2). The calculated amount of the 2M N-doped sample is $0.049 mF.cm^{-2}$. In comparison, the resulting amount for the 0.5, 1, 4 and 8 molar are 0.022, 0.033, 0.031 and 0.019 $mF.cm^{-2}$ respectively.

Galvanostatic charge/discharge curves of the samples at a current density of $50 \mu A$ are shown in fig. 2b. It can be noticed that all of the curves have a linear and roughly symmetric shape which serves as further evidence of desirable capacitance behavior. Consistent with the EIS and CV results, the 2M N-doped sample shows a higher capacitance regarding the larger area at the same current density ($50 \mu A$). As for the result of EIS, CV, and charge dis-charge tests of 0.5, 1, 2, 4, 8M N-doped samples, the sample immersed in 2 M ammonia solution exhibited the highest capacitance operation.

Table 2- The fitting values obtained from the equivalent circuit for TNT, N-TNT, R-TNT, and R-N-TNT samples

sample	TNT	N-TNT	R-TNT	R-N-TNT
R1($\Omega.cm^{-2}$)	6.218	7.045	4.979	6.018
CPE1-T($mFs^{p-1}.cm^{-2}$)	3.59E-6	8.5065E-6	0.036958	0.40658
CPE1-P	0.90979	0.9197	0.621	0.3282
Rct($\Omega.cm^{-2}$)	2398	76.2	2.567	0.63309
W-R($\Omega.cm^{-2}$)	7931	1024	0.0035514	5.583
W-T	1804	0.44495	6.8201E-5	0.0034869
W-P	0.51384	0.37541	0.4816	4.989
R3($\Omega.cm^{-2}$)	-	-	46684	14770
C1($mFs^{p-1}.cm^{-2}$)	-	-	0.0059024	-
CPE2-T($mFs^{p-1}.cm^{-2}$)	-	-	-	0.0082247
CPE2-P	-	-	-	0.98511

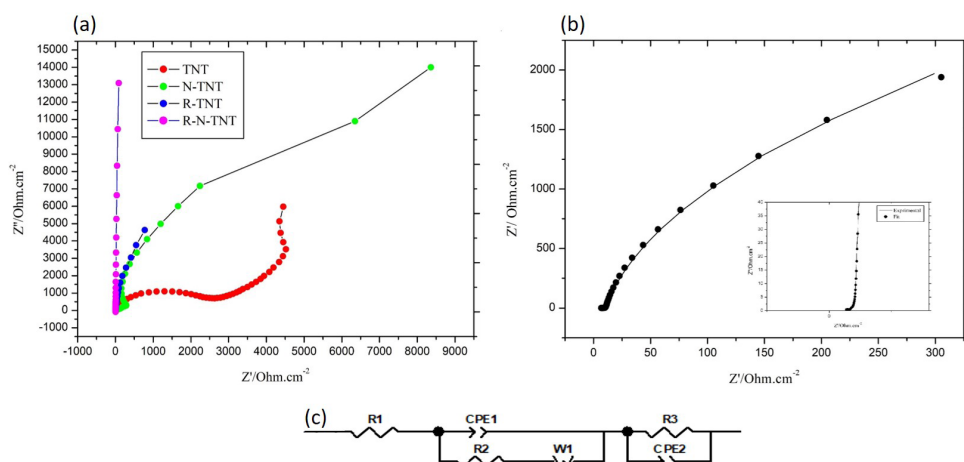


Fig. 3- Nyquist representation of (a) TNT, N-TNT, R-TNT, and R-N-TNT (b)R-N-TNT, (c) the applied equivalent circuit.

Therefore, the electrochemical doping process was performed on the 2M N-doped sample for further improvement of capacitance behavior. The EIS, CV and galvanostatic charge discharge tests repeated on optimized samples.

Table 2 lists the quotative analysis parameter of impedance for TNT, N-TNT, R-TNT, and R-N-TNT samples. As can be seen, the CPE parameter (Helmholtz double-layer capacitance) is increased. Simultaneously, R_{ct} is decreased from 2398 $\Omega.cm^{-2}$ for TNT to 76.2 $\Omega.cm^{-2}$ for N-TNT, 2.567 $\Omega.cm^{-2}$ for R-TNT and 0.63309 $\Omega.cm^{-2}$ for R-N-TNT. Both nitrogen and electrochemical doping provide easier access for charge transfer and lower resistance of the TNT [27]. Therefore, when both these methods of improvement are employed, conductivity and capacitance operation show outstanding progress.

Fig. 3a represents the EIS plots of TNT, N-TNT, R-TNT, and R-N-TNT samples to compare capacitance and charge transport behavior at the electrode-electrolyte interface of the electrodes. As expected, the shape of the impedance plots consists

of incomplete semicircles in the high-frequency region, and an inclined line at an approximate 75° to 80° angle with the low-frequency region, which can be attributed to charge transfer behavior and electron diffusion processes, respectively. However, the impedance plot for the R-N-TNT electrode features an almost vertical line at lower frequencies, which stands for ideal capacitor characteristics. For a detailed observation, the Nyquist representation of R-N-TNT as the high-efficiency sample is presented in Fig. 3b. The applied equivalent circuit used in the simulation of quantitative values for EIS of R-TNT and R-N-TNT sample is shown in Fig. 3c. It is worth noting that for TNT and N-TNT, the equivalent circuit brought at Fig. 1c was used.

Fig. 4a represents the comparative CV curves of TNT, N-TNT, R-TNT and R-N-TNT. For faradic mechanisms; showing an almost rectangular shape demonstrate a suitable charge propagation within the electrodes for all samples except TNT. The shape of the CV curve of the TNT sample is roughly triangular which represents the manner of

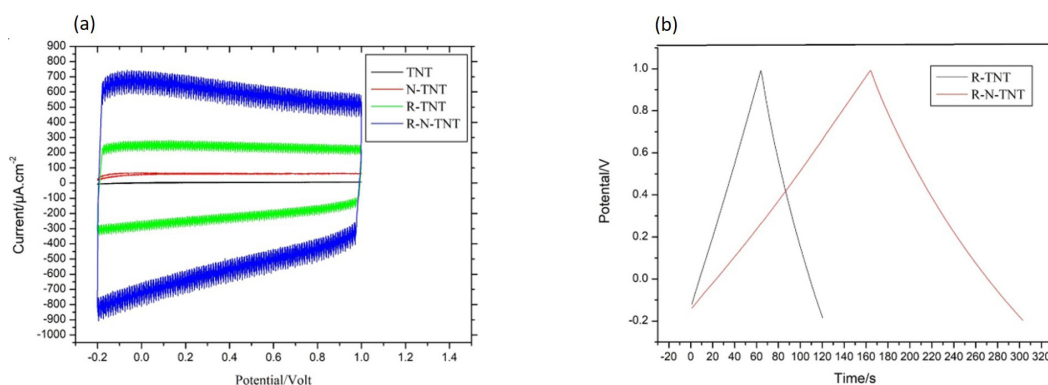


Fig. 4- (a) CV curves of TNT, N-TNT, R-TNT and R-N-TNT and (b) galvanostatic charge/discharge curves of R-TNT and R-N-TNT.

semiconduction and shows a strong dependence of current density on potential. The CV curve of R-T-TNT exhibits a larger integrated area and higher current response, representing a noticeable enhancement in capacitance performance after the nitrogen and electrochemical doping process. A nearly rectangular shape with no identifiable redox peaks is a clear sign of double-layer capacitance characteristic.

The values of the areal capacitance obtained from CV curves at 100 mA.cm^{-1} using equation (1-1) for TNT, N-TNT, R-TNT and R-N-TNT are 0.0271, 0.0492, 6.308 and $11.5833 \text{ mF.cm}^{-2}$, respectively, proves the excellent improvement of capacitance behavior for R-N-TNT.

Fig. 4b compares the charge dis-charge performance of R-TNT and R-N-TNT samples. The fully symmetrical charge discharge curves demonstrate the good coulombic efficiency of the samples. As predictable, the R-N-TNT sample indicates a longer charge/discharge time. According to equation (2), the areal capacitance of the samples per charge/discharge curves can be measured as follows [22]:

$$C_s = I \times \Delta t / (S \times \Delta V) \quad (2)$$

In which C_s is the areal capacitance (mF.cm^{-2}), I is the discharge current (A), Δt the discharge time(s), S is the surface area of the working electrode (cm^2), and V is the potential, respectively. The obtained value for R-TNT is 2.33 mF.cm^{-2} and 5.79 mF.cm^{-2} for R-N-TNT revealing the positive effective of simultaneous nitrogen application and electrochemical doping. It should be noted that TNT and N-TNT samples have certain limitations when it comes to applied current density, and face operation problems at high current density. They

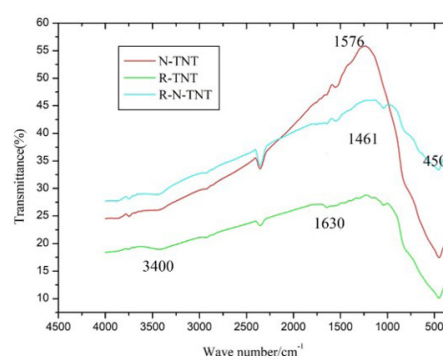


Fig. 5- FTIR spectrum of TNT, N-TNT, R-TNT and R-N-TNT samples.

suffer from a sizeable voltage at the beginning of discharge [24].

Fig. 5 illustrates the FT-IR spectrum of TNT, N-TNT and R-N-TNT which can provide the information on the functional groups located on the surface of materials. Apparent peaks at 3400, 1630 and 450 cm^{-1} present in all samples can be ascribed to the stretching vibration of $-\text{OH}$, the bending vibration of $\text{H}-\text{O}$ bond and the vibration of $\text{Ti}-\text{O}-\text{Ti}$ bond, respectively. In the case of N-TNT and R-N-TNT samples, a new peak is observed at around 1461 cm^{-1} observed which can be may be assigned to the N-H bending, representing successful doping of nitrogen atoms. Another peak also at 1576 cm^{-1} could be assigned to the surface adsorbed of N-O which was not detected for the R-TNT sample [29, 30, 31].

The FESEM image, XRD patterns, and EDS results of TNT following immersion at 2 M ammonia solution for 15 hours before electrochemically doping reaction are presented in Fig. 6. In the top view of the FESEM image (Fig. 4a), a highly ordered morphology with high density

Table 3- Quantitative values resulted from EDS test of R-N-TNT

Elt	Line	Int	Error	K	Kr	W%	A%	ZAF	Ox%	Pk/Bg	LConf	HConf
C	Ka	47.0	3.2542	0.0369	0.0211	4.38	8.54	0.4815	0.00	6.10	3.98	4.78
N	Ka	60.2	3.2542	0.0609	0.0349	5.61	9.38	0.6220	0.00	8.00	5.15	6.06
O	Ka	252.8	3.2542	0.1138	0.0651	39.02	57.14	0.1669	0.00	43.71	37.48	40.57
Ti	Ka	1454.5	1.0643	0.7884	0.4512	50.99	24.94	0.8850	0.00	56.80	50.15	51.83
				1.0000	0.5723	100.0	100.0		0.00			

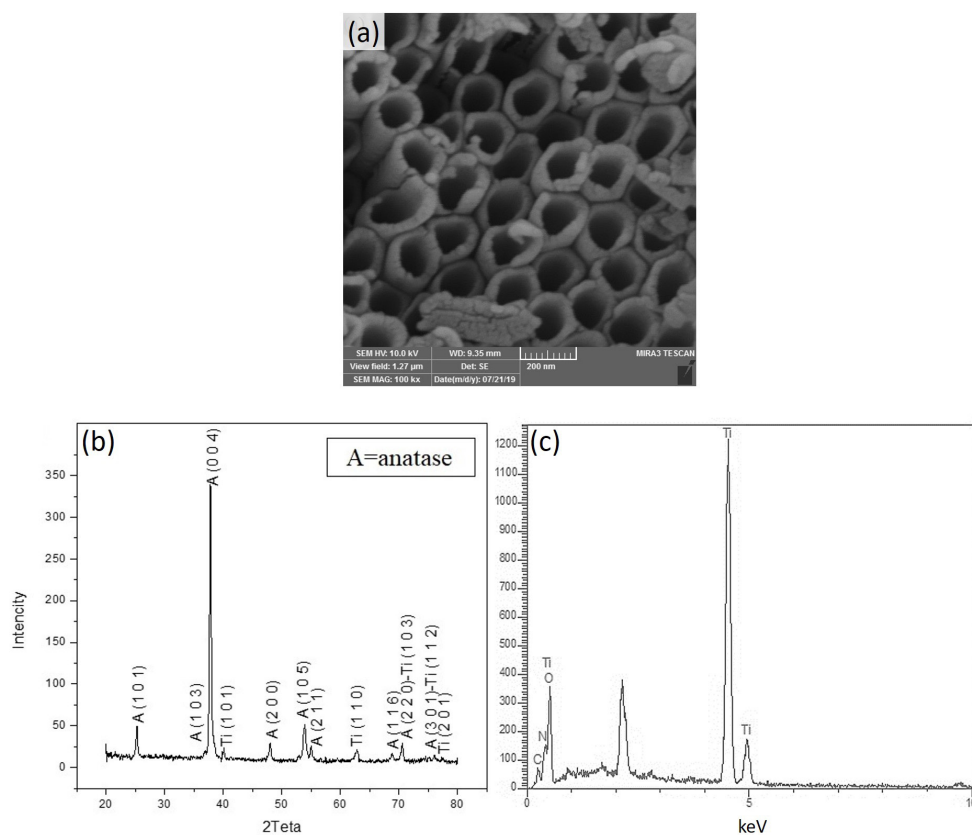


Fig. 6- (a) FESEM image, (b) XRD, and (c) EDS result of the R-N-TNT sample.

and a uniform characteristic can be observed. The nanotubes with glossy walls and homogeneous dimensions were aligned vertically on the Ti substrate. XRD analysis was carried out to study the crystal structure of the R-N-TNT (Fig. 4b). Except for the peaks located at (112), (103), (110), and (201) plates which originate from the Ti metal substrate, all other peaks can be readily indexed to anatase TiO_2 . Therefore, R-N-TNT represents the developed anatase phase with a high degree of crystallinity. Based on the EDS results, Ti, C, N, and O are the main substances observed in the structure of the R-N-TNT sample along with 39.02 wt% O, 5.61 wt% N, and 4.38 wt% C, revealing the successful nitrogen and electrochemical doping process (Table 3).

Fig. 7a indicates the CV curves of the R-N-TNT

sample obtained at various ranges of scanning rates (10, 20, 30, 50, 100, 200 $\text{mV}\cdot\text{s}^{-1}$). As can be seen, CV curves retain their rectangular shape even at higher scanning rates, which can be interpreted as a sign of high rate capability and capacitance behavior. The improved rate capacitance of the R-N-TNT electrode was mainly ascribed to the superior conductivity. The areal capacitances derived from the CV curves are plotted in Fig. 7b. As the scanning rate is increased from 10 to 200 $\text{mV}\cdot\text{s}^{-1}$, areal capacitance is dropped from 8.75 to only 7.8 $\text{mV}\cdot\text{s}^{-1}$; with an 89% retention of initial capacitance, indicating a desirable high-rate capacitive behavior.

Fig. 7c shows the galvanostatic charge/discharge measurements of the R-N-TNA conducted under different current densities (50, 75, 100, 150, 200, 300 $\mu\text{A}\cdot\text{cm}^{-2}$), conforming steadily operation

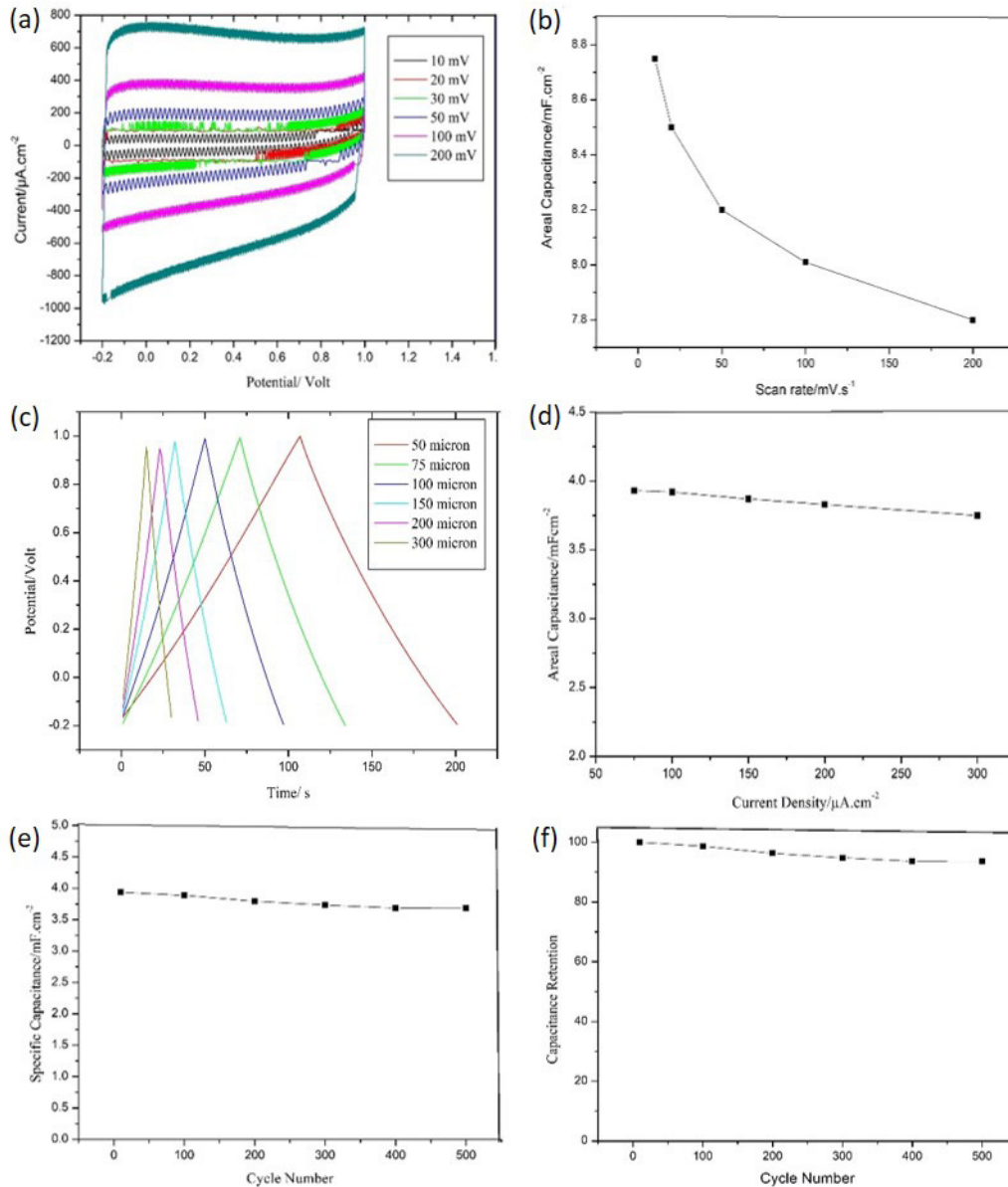


Fig. 7- (a) CV curves obtained at various range of scanning rates (10, 20, 30, 50, 100, 200 mV.s⁻¹), (b)) the areal capacitance of the R-N-TNT sample obtained from CV, (c) galvanostatic charge/discharge curves at different current densities (50, 75, 100, 150, 200, 300 μA.cm⁻²), (d) the areal capacitance of the R-N-TNT sample obtained from galvanostatic charge/discharge curves, (e) specific capacitance measured at 100 μA.cm⁻² under 500 cycles, and (f) capacitance retention of R-N-TNT sample after 500 cycles.

over a wide range of current densities. The nearly symmetrical charge/discharge curves at various current densities demonstrate good coulombic efficiency. As current density is increased from 50 to 300 μA.cm⁻², voltage and charge/discharge time demonstrated a linear relationship, confirming the non-faradic capacitive behavior and good rate capability. Fig. 7d shows the capacitance of the optimal sample in terms of current density. With increasing current density, there are no significant

changes in capacitance (3.9 mF.cm⁻² for 75 μA.cm⁻² and 3.7 mF.cm⁻² for 300 μA.cm⁻²), which is also in confirmation of the high-rate capacitive behavior. Fig. 7e depicts the areal capacitance of the optimal sample measured at 100 μA.cm⁻² during 500 cycles. Fig. 7f shows the capacitance retention calculated with the help of the data from Fig. 7e. R-N-TNT electrode exhibits long-term stability with 93% of its initial capacitance after 500 cycles, suggesting a relatively good long-term cycling stability.

4. Conclusion

To summarize, both nitrogen doping and electrochemical reduction techniques were utilized to improve the weak capacitance behavior of TNT. Given the importance of the number of nitrogen particles on the capacitance performance of nanotubes, N-TNT samples were synthesized at various levels of concentration. As the result of EIS, CV, and charge/discharge tests would suggest, the sample with 2M density showed the optimal properties. Following the electrochemical reduction of the 2M N-doped sample, a significant improvement in capacitance performance was obtained. According to the data derived from EIS analysis, interface charge transfer resistance (R_{ct}) was decreased from $2398 \Omega \cdot \text{cm}^{-2}$ (for TNT) to $0.63309 \Omega \cdot \text{cm}^{-2}$ (for R-N-TNT), leading to a drop in electron transfer resistance. Regarding the areal capacitance CV curves of $100 \text{ mV} \cdot \text{s}^{-1}$ scanning rate, the areal capacitance calculated for R-N-TNT with the help of CV curves was about 2 orders of magnitude greater than that of R-TNT, and roughly 400 orders of magnitude greater than TNT. Furthermore, CV curves of R-N-TNT represent an almost ideal capacitive shape even at a high scanning rate of $200 \text{ mV} \cdot \text{s}^{-1}$. With the application of different discharge current densities, the areal capacitance of the R-N-TNT sample was slightly reduced, which demonstrates the high-rate capacitive behavior.

It can be deduced that both the nitrogen doping process and electrochemical reduction can enhance the conductivity and capacitive performance of TNT. However, when both these methods are employed simultaneously, the capacitance performance is improved dramatically.

References

- Raj CC, Prasanth R. Review—Advent of TiO₂Nanotubes as Supercapacitor Electrode. *Journal of The Electrochemical Society*. 2018;165(9):E345-E58.
- Samsudin NA, Zainal Z, Lim HN, Sulaiman Y, Chang SK. Titania nanotubes synthesised via the electrochemical anodisation method: Synthesis and supercapacitor applications. *Pertanika Journal of Scholarly Research Reviews*. 2016;2(1).
- Gamby J, Taberna PL, Simon P, Fauvarque JF, Chesneau M. Studies and characterisations of various activated carbons used for carbon/carbon supercapacitors. *Journal of Power Sources*. 2001;101(1):109-16.
- Bai Y, Rakhi RB, Chen W, Alshareef HN. Effect of pH-induced chemical modification of hydrothermally reduced graphene oxide on supercapacitor performance. *Journal of Power Sources*. 2013;233:313-9.
- Kiamahalleh MV, Zein SHS, Najafpour G, Sata SA, Buniran S. MULTI-WALLED CARBON NANOTUBES BASED NANOCOMPOSITES FOR SUPERCAPACITORS: A REVIEW OF ELECTRODE MATERIALS. *Nano*. 2012;07(02):1230002.
- Samsudin NA, Zainal Z, Lim HN, Sulaiman Y, Chang SK. Titania nanotubes synthesised via the electrochemical anodisation method: Synthesis and supercapacitor applications. *Pertanika Journal of Scholarly Research Reviews*. 2016;2(1).
- Jang K, Yu S, Park S-H, Kim H-S, Ahn H. Intense pulsed light-assisted facile and agile fabrication of cobalt oxide/nickel cobaltite nanoflakes on nickel-foam for high performance supercapacitor applications. *Journal of Alloys and Compounds*. 2015;618:227-32.
- Inamdar AI, Kim Y, Pawar SM, Kim JH, Im H, Kim H. Chemically grown, porous, nickel oxide thin-film for electrochemical supercapacitors. *Journal of Power Sources*. 2011;196(4):2393-7.
- Wei W, Cui X, Chen W, Ivey DG. Manganese oxide-based materials as electrochemical supercapacitor electrodes. *Chem Soc Rev*. 2011;40(3):1697-721.
- Chuang C-M, Huang C-W, Teng H, Ting J-M. Effects of Carbon Nanotube Grafting on the Performance of Electric Double Layer Capacitors. *Energy & Fuels*. 2010;24(12):6476-82.
- Wang Z, Cao D, Xu R, Qu S, Wang Z, Lei Y. Realizing ordered arrays of nanostructures: A versatile platform for converting and storing energy efficiently. *Nano Energy*. 2016;19:328-62.
- Chen H. Hydrothermal Synthesis and Electrochemical Properties of TiO₂ Nanotubes as an Anode Material for Lithium Ion Batteries. *International Journal of Electrochemical Science*. 2018;2118-25.
- Salari M, Konstantinov K, Liu HK. Enhancement of the capacitance in TiO₂ nanotubes through controlled introduction of oxygen vacancies. *Journal of Materials Chemistry*. 2011;21(13):5128.
- Bendavid A, Martin PJ, Jamting Å, Takikawa H. Structural and optical properties of titanium oxide thin films deposited by filtered arc deposition. *Thin Solid Films*. 1999;355-356:6-11.
- Chen X, Shen S, Guo L, Mao SS. Semiconductor-based Photocatalytic Hydrogen Generation. *Chemical Reviews*. 2010;110(11):6503-70.
- Mali SS, Shim CS, Kim H, Patil PS, Hong CK. In situ processed gold nanoparticle-embedded TiO₂nanofibers enabling plasmonic perovskite solar cells to exceed 14% conversion efficiency. *Nanoscale*. 2016;8(5):2664-77.
- Shinde PS, Patil PS, Bhosale PN, Brüger A, Nauer G, Neumann-Spallart M, et al. UVA and solar light assisted photoelectrocatalytic degradation of AO7 dye in water using spray deposited TiO₂ thin films. *Applied Catalysis B: Environmental*. 2009;89(1-2):288-94.
- Patil JV, Mali SS, Kamble AS, Hong CK, Kim JH, Patil PS. Electrospinning: A versatile technique for making of 1D growth of nanostructured nanofibers and its applications: An experimental approach. *Applied Surface Science*. 2017;423:641-74.
- Roy P, Berger S, Schmuki P. TiO₂ Nanotubes: Synthesis and Applications. *Angewandte Chemie International Edition*. 2011;50(13):2904-39.
- Mu Jo S, Yeon Song M, Rack Ahn Y, Rae Park C, Young Kim D. Nanofibril Formation of Electrospun TiO₂Fibers and its Application to Dye-Sensitized Solar Cells. *Journal of Macromolecular Science, Part A*. 2005;42(11):1529-40.
- Lu X, Wang G, Zhai T, Yu M, Gan J, Tong Y, et al. Hydrogenated TiO₂ Nanotube Arrays for Supercapacitors. *Nano Letters*. 2012;12(3):1690-6.
- Chen J, Xia Z, Li H, Li Q, Zhang Y. Preparation of highly capacitive polyaniline/black TiO₂ nanotubes as supercapacitor electrode by hydrogenation and electrochemical deposition. *Electrochimica Acta*. 2015;166:174-82.

23. Zheng Z, Huang B, Qin X, Zhang X, Dai Y, Whangbo M-H. Facile in situ synthesis of visible-light plasmonic photocatalysts M@TiO₂ (M = Au, Pt, Ag) and evaluation of their photocatalytic oxidation of benzene to phenol. *Journal of Materials Chemistry*. 2011;21(25):9079.
24. Chen X, Mao SS. Titanium Dioxide Nanomaterials: Synthesis, Properties, Modifications, and Applications. *Chemical Reviews*. 2007;107(7):2891-959.
25. Azami MS, Nawawi WI, Jawad AH, Ishak MAM, Ismail K. N-doped TiO₂ Synthesised via Microwave Induced Photocatalytic on RR4 dye Removal under LED Light Irradiation. *Sains Malaysiana*. 2017;46(8):1309-16.
26. Wu H, Li D, Zhu X, Yang C, Liu D, Chen X, et al. High-performance and renewable supercapacitors based on TiO₂ nanotube array electrodes treated by an electrochemical doping approach. *Electrochimica Acta*. 2014;116:129-36.
27. Peighambardoust NS, Khameneh Asl S, Mohammadpour R, Asl SK. Band-gap narrowing and electrochemical properties in N-doped and reduced anodic TiO₂ nanotube arrays. *Electrochimica Acta*. 2018;270:245-55.
28. Lai L, Yang H, Wang L, Teh BK, Zhong J, Chou H, et al. Preparation of Supercapacitor Electrodes through Selection of Graphene Surface Functionalities. *ACS Nano*. 2012;6(7):5941-51.
29. Geng J, Yang D, Zhu J, Chen D, Jiang Z. Nitrogen-doped TiO₂ nanotubes with enhanced photocatalytic activity synthesized by a facile wet chemistry method. *Materials Research Bulletin*. 2009;44(1):146-50.
30. Tran VA, Truong TT, Phan TAP, Nguyen TN, Huynh TV, Agresti A, et al. Application of nitrogen-doped TiO₂ nanotubes in dye-sensitized solar cells. *Applied Surface Science*. 2017;399:515-22.
31. Peighambardoust NS, Khameneh Asl S, Maghsoudi M. The effect of doping concentration of TiO₂ nanotubes on energy levels and its direct correlation with photocatalytic activity. *Thin Solid Films*. 2019;690:137558.